Nanoscale

Accepted Manuscript

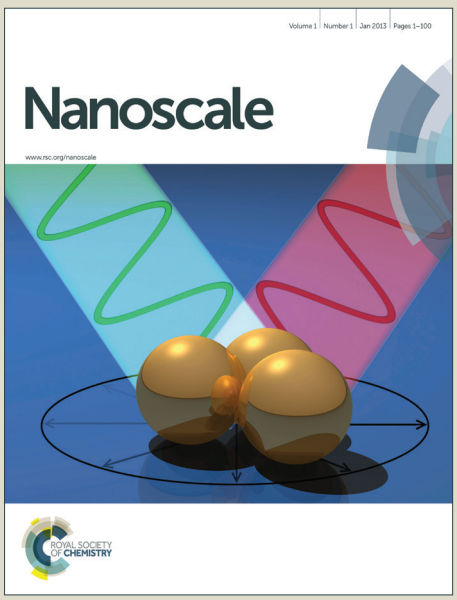

ROYAL SOCIETY OF CHEMISTRY

www.rsc.org/nanoscale

Impedance spectroscopic analysis on effects of partial oxidation of TiN bottom electrode and microstructure of amorphous and crystalline HfO_2 thin films on their bipolar resistive switching

Ji-Wook Yoon,[a] Jung Ho Yoon,[b] Jong-Heun Lee[a,c#] and Cheol Seong Hwang[b*]

[a]Department of Materials Science and Engineering, Korea University, Anam-Dong, Sungbuk Gu, Seoul 136-714, Republic of Korea

[b]Department of Materials Science and Engineering, and Inter-university Semiconductor Research Center, Seoul National University, Seoul 151-744, Korea

[c]Department of Nano-Semiconductor Engineering, Korea University, Anam-Dong, Sungbuk Gu, Seoul 136-714, Republic of Korea

The electrical resistance switching (RS) properties of amorphous HfO_2 (a-HfO_2) and crystalline HfO_2 (c-HfO_2) thin films grown on a TiN substrate via atomic layer deposition were examined using DC current-voltage (I-V) sweep and AC impedance spectroscopic (IS) analyses. The rapid thermal annealing of the a-HfO_2 film at 500°C under a N_2 atmosphere for 5 min crystallized the HfO_2 film and induced an interfacial TiON barrier layer. The a-HfO_2 sample showed fluent bipolar RS performance with a high on/off ratio (~500), whereas the c-HfO_2 sample showed a much lower on/off ratio (<~10), but its switching uniformity was better than that of a-HfO_2. Such critical differences can be mainly attributed to the absence and presence of the TiON barrier layer in the a-HfO_2 and c-HfO_2 samples, respectively. The AC IS especially enabled the resistance states of the HfO_2/Pt interface and the HfO_2/TiN interface to be separately examined during one complete switching cycle of each sample. Although the Pt/c-HfO_2 interface has Schottky barrier at the pristine state, it disappears once the c-HfO_2 is electroformed and was not recovered even after the reset step. In contrast, the Pt/a-HfO_2 interface recovers partly the Schottky barrier after the reset.

Corresponding author E-mail: jongheun@korea.ac.kr
* Corresponding author E-mail: cheolsh@snu.ac.kr

I. Introduction

HfO_2 thin films play a crucial role in modern semiconductor devices as a high-*k* gate dielectric layer in the metal insulator semiconductor field effect transistor due to its higher *k* value compared with the conventional SiO_2 as well as its sufficiently high energy gap.[1] They recently became another class of important material for the resistance switching random access memory (RRAM), showing fluent resistance switching (RS) performances.[2-5] Apart from other RS oxide materials that have a distinctive conducting phase when electro-reduced, such as the Magnéli phase in TiO_2,[6-7] HfO_2 does not have any distinctive second phase in its phase diagram. As such, RS is believed to be related with the formation of oxygen vacancies and their percolation to form the conducting path in its low resistance state (LRS) while the high resistance state (HRS) is induced by the disruption of such conduction paths.[8-11] The control of the oxygen vacancy concentration and their percolation on the atomic level makes multi-level switching feasible as well.[12] The influence of the microstructure (amorphous or crystalline) on the RS performance of the HfO_2, however, is not clearly understood even though the oxygen vacancy formation and percolation must have a close correlation with the microstructure.

The electrodes in the RRAM also play a crucial role not only as electrodes but also as the sources and sinks of oxygen vacancies (or oxygen ions).[3] Sometimes, the interfaces between the electrode and HfO_2 work as the source and sink of the oxygen vacancies.[13] Balatti et al. recently reported that the appropriate control of voltage pulses applied to the thin HfO_x layer sandwiched between the TiN top and bottom electrodes could induce the complementary-type resistance switching.[14] TiN is an important electrode and diffusion barrier material in semiconductor memory and logic devices. For RRAM application, TiN appears to have desirable properties because it maintains feasible electrical conductivity even with a quite high oxygen concentration in it.[15] Furthermore, the lower effective work function of TiN (~4.6 eV) on HfO_2 (Ref. 16) compared to that of Pt (~5.5 eV) makes the TiN/HfO_2 junction much more carrier-(electron)-injecting than the Pt/HfO_2 interface. Therefore, TiN/HfO_2/Pt can constitute a feasible bipolar resistance switching (BRS) system, in which the modulation of the Schottky barrier (SB) at the HfO_2/Pt interface by the accumulation and depletion of oxygen vacancies according to the applied bias polarity are supposed to induce the BRS behavior. However, it was found in this work that this is true only for the case of amorphous HfO_2, whereas a completely different BRS mechanism was found for crystalline HfO_2 once it was electroformed. It has to be noted that the SB-modulation related BRS does not necessarily coincide with the area-type switching; it can be occurred at local positions along the interface between oxide film and electrode.

Determining the exact mechanism for RS in such system has been a tough task, however, when the systems have only atomic-level changes during the switching operation, which cannot be

clearly identified even with high resolution transmission electron microscopy (HRTEM). The point-defect-like nature of the vacancies renders their observation in spatial dimensions very challenging even in HRTEM, and only spectroscopic analysis can indirectly supplement the electrical results. Moreover, the elucidation of RS mechanism based on spectroscopic analysis is still difficult due to highly localized nature and low density of the conduction channel (percolating path) even in the LRS. Therefore, to the authors' knowledge, there has been a scarcity in reports directly correlating electrical RS and the structural or chemical changes in the HfO_2 RRAM system.

In this work, a controlled set of experiments was performed to determine the correlation between the structure and electrical properties of the TiN/HfO_2/Pt RS system by depositing an 11.3-nm-thick HfO_2 film on a sputtered 100-nm-thick TiN electrode via atomic layer deposition (ALD), and the microstructure and crystallinity of the dielectric film were varied through thermal annealing. The as-deposited HfO_2 film was amorphous (a-HfO_2), but the annealed film showed a crystalline microstructure with a monoclinic phase (c-HfO_2). While these two types of films have a common TiN bottom electrode (BE) and a common Pt top electrode (TE), they showed quite distinctive RS properties in the repeated DC current-voltage (I-V) sweep. The depth profiling using X-ray photoelectron spectroscopy (XPS) revealed that the HfO_2/TiN interface in c-HfO_2 became to have a TiON barrier layer through thermal annealing, which was confirmed by cross-sectional TEM, while a-HfO_2 did not show such barrier layer. The primary merit of the present work lies in the extensive use of impedance spectroscopy (IS) for both samples to examine the various electrical states of the samples during the electrical switching. IS has been already used to examine the RS behaviors of TiO_2,[17,18] NiO,[18,19] and HfO_2.[18] While the NiO films show metallic behaviors and parallel circuit components composed of resistance (R) and capacitance (C) in LRS and HRS, respectively, in both Refs. 18 and 19, TiO_2 film showed different states of LRS depending on the switching mode. When it is under the LRS of unipolar RS (URS) with Pt film being as the top and bottom electrodes, due to the presence of strong Magnéli phase filament, no C component was found, while the HRS clearly showed the parallel RC circuit component.[17] In contrast, when the TiO_2 film is under the BRS mode with indium tin oxide being as the top and bottom electrodes, which perhaps precludes the formation of strong Magnéli phase filament, both LRS and HRS showed parallel RC circuit components, which were ascribed to the different degree of filament rupture.[19] Two HfO_2 films grown by sputtering and pulsed laser deposition also showed disparate status of LRS, where the sputtered film showed metallic conduction and pulsed laser deposited film showed RC components.[18] All these detailed analyses demonstrate the usefulness of IS in revealing the underlying microscopic mechanism of RS in various oxide films. However, detailed IS study on HfO_2 having different microstructures has not been reported yet. The alternating current (AC) IS allowed the identification of the electrical states of the interface with the electrodes separately from that of the bulk HfO_2, which greatly contributed to the

improved understanding of the RS mechanisms of the two samples. Memory cells with a lateral dimension of as small as 10 x 10 nm^2 using Hf/HfO_2 bi-layer structure as the active RS element with TiN electrodes have been reported.[3] The amorphous HfO_2 film was deposited by an ALD technique and post-deposition annealing at 600 ^oC under N_2 atmosphere was used to examine the effect of crystallization of the dielectric film.[3] It was reported that the RS could be ascribed to the localized formation and rupture of conducting filament(s) down to the smallest cell area (10 x 10 nm^2) in both the amorphous and crystalline HfO_2. However, IS was not adopted in that report.

In this work, the microscopic-level changes such as the dynamic evolutions in conducting filament, interfacial TiON region, and matrix phase during the various steps of the RS were systematically studied using AC IS. This cannot be achieved through the DC electrical test because the DC measurement gives the overall resistance in any electrical state. It was determined that the formation of an interfacial TiON region critically influences the RS performances. As such, controlling this layer is very important in RRAM fabrication, using the TiN layer as the electrode.

II. Experimental section

Using an 8-inch-diameter-scale traveling-wave-type ALD reactor (CN-1 Co. Plus 200), 11.3-nm-thick HfO_2 films were deposited on a 100-nm-thick TiN/Si wafer, where the TiN wafer the reactively sputter-deposited using a commercial sputtering system (Endura, Applied Materials). The native oxide on the Si wafer surface was removed through a standard Radio Corporation of America cleaning process prior to the deposition of the TiN film. ALD of the HfO_2 film was performed using the $Hf[N(CH_3)(C_2H_5)]_4$ and O_3 as the Hf-precursor and oxygen source, respectively. The Hf precursor and O_3 pulse durations were 2 and 3 s, respectively, and Ar purge gas was injected for 9 and 3 s, respectively, after each of these two chemical pulses. The wafer temperature during the deposition was set to 280^oC. A part of the as-deposited sample was post-annealed at 500^oC for 5 min under a N_2 atmosphere, using a rapid thermal annealing equipment for crystallization. The film thickness, microstructure, surface topography, local electrical conduction, and chemical status of the films were examined via spectroscopic ellipsometry (Ellipso Technology Co., Ltd.), X-ray diffraction (XRD, D/MAX-2500V/PC, Rigaku), conductive atomic force microscopy (CAFM, JEOL JSPM 5200), and XPS (ThermoVG, Sigma Probe), respectively. The cross-section of the a-HfO_2 and c-HfO_2 samples were observed using a HRTEM (JEOL 3000F at 300 keV). For electrical measurement, top electrodes with areas ranging from 5 x 10^3 to 1 x 10^6 μm^2 were fabricated by lift-off process using electron-evaporated Pt film. Most electrical tests were performed on the electrodes with an area of ~ 7 x 10^4 μm^2. DC electrical test was performed using a Keithley 2400 voltage source meter and HP 4155B semiconductor parameter analyzer. Impedance characterizations were performed using an impedance analyzer (Alpha-N, Novocontrol) from 0.1 to 10^7 Hz, and the voltage amplitude of the impedance spectroscopy was 100 mV. All the electrical tests were performed at room temperature with the Pt top

electrode being biased and the bottom TiN electrode being grounded. The contribution of lead wire resistance was confirmed to be negligible in the analysis by measuring the resistance in short-circuit condition.

III. Results and Discussion

Structural characterization of a-HfO_2 and c-HfO_2 thin films

The XRD spectra in 2θ mode of the TiN BE, 11.3-nm-thick a-HfO_2, and c-HfO_2 films are shown in Figures 1a-c, respectively. The TiN film was crystallized with the cubic rock salt structure, and the a-HfO_2 film was amorphous while the c-HfO_2 film was crystallized into the monoclinic structure. Figures 1d and e show topographic AFM images of the 11.3-nm-thick a-HfO_2 and c-HfO_2 films, respectively. Figures 2a and b show the topographic AFM images of the 5.5-nm-thick a-HfO_2 and c-HfO_2 films, respectively. Although majority of the switching experiments were performed with 11.3-nm-thick HfO_2 films, a thinner film was adopted for the CAFM because the thicker film was too insulating to achieve measureable current images. The root-mean-squared (RMS) roughness of the 5.5 (11.3)-nm-thick a-HfO_2 film was 0.18 (0.49) nm, which increased to 0.32 (0.73) nm in the c-HfO_2 film due to the crystallization and interfacial TiON layer formation. Figures 2c and d show the CAFM images of the two types of HfO_2 films when the Pt/Ir-coated tip was grounded and the TiN bottom electrode was positively biased with 2.5 V. The a-HfO_2 film showed rather uniform current flow across the scanned area except for several spatial locations where current level is much lower, which is consistent with the amorphous structure of this sample. (Note that higher current corresponds to lower value in y-axis which is due to the specific program of this CAFM system) In contrast, the c-HfO_2 film showed a localized current flow mainly along the grain boundaries of the c-HfO_2 film (compared with the topographic image). Figures 2e, f show the cross-sectional images of Figures 2a, c and 2b, d, respectively, indicated by red bands, which even more clearly show the correlations. This must be related with the more defective nature of the grain boundary region compared with the stoichiometric grain regions in the c-HfO_2 film. These differences in the current flow pattern of pristine HfO_2 films (films before RS operations) greatly influence the mechanism for RS, as discussed in detail below.

Figure 3 shows the XPS depth profile results of the two samples. For the XPS experiment, the Ar^+ beam energy was set to 1 keV to minimize the sputtering damage, and the core level spectra of (a) Ti *2p*, (b) N *1s*, (c) Hf *5f*, and (d) O *1s* were monitored. Here, the time between the etch levels was 10 s. Ti and N signals were begun to be seen from the 7^{th} and 8^{th} spectra for the a-HfO_2 and c-HfO_2 films, respectively (Figures 3a, b). The binding energies (BEs) of the Ti and N core levels shifted into a higher BE direction in the c-HfO_2 film compared with the a-HfO_2 film. These results indicate that the TiON interfacial layer is formed during annealing. The O/Hf ratio for the 1^{st}-4^{th} spectra of Figures

3c, d calculated from the peak area and sensitivity factors shows no notable difference between the two samples. The BEs of the Hf and O peaks from the c-HfO_2 film, however, show opposite shifts relative to those from the a-HfO_2 film. The difference between the BEs of the O and Hf peaks of both samples (513.6 eV for the a-HfO_2 film and 514.5 eV for the c-HfO_2 film) were higher than the reported value for bulk HfO_2 (512.4 eV),[20] suggesting a rather high deviation of the chemical states from the equilibrium, which is understandable considering the thin-film structure of the materials. A more notable finding is that the evident O *1s* peak was observed even on levels 8-11 (Figure 3d), suggesting serious oxygen diffusion into the TiN layer. The O peak intensity on these levels was certainly higher in the c-HfO_2 film than in the a-HfO_2 film, corroborating the higher oxidation of TiN in the c-HfO_2 case. The presence of the TiON regions in the case of the c-HfO_2 film was also confirmed by cross-sectional TEM, which also confirmed the amorphous (Figures 4a, c) and crystalline (Figures 4b, d) structures of a-HfO_2 and c-HfO_2 films, respectively. Cross-sectional TEM revealed that the TiON regions are rather locally formed mainly at grain boundary regions of the TiN electrode, and non-oxidized TiN grains improve their crystalline quality. Confirmation of chemical composition (O/N ratio) of the amorphous-like and crystalline regions in the interfacial Ti(O)N layer by the energy dispersive spectroscopy in the TEM was not possible due to the presence of oxide scales on both sides of the TEM samples. Therefore, changes in the chemical state by annealing must be understood from the XPS depth profile results. This TiON-rich interface region is represented as TiON layer in this report.

I-V characteristics

As the pristine a-HfO_2 and c-HfO_2 films are highly electrically insulating at their pristine states, an appropriate electroforming step was necessary to induce a reliable RS. Electroforming could be achieved by both the positive and negative bias polarities, but the electroformed samples with the positive bias showed reliable switching cycle numbers of only 10 to 20 for both samples. Top Pt electrode was biased while bottom TiN electrode was grounded during all the electrical measurements. Therefore, the samples electroformed with the negative bias were adopted for a further test in this work. Figures 5a, b show the electroforming I-V curves of the a-HfO_2 and c-HfO_2 films, respectively, and the subsequent first BRS-type switching curves. The electroforming voltages for the a-HfO_2 and c-HfO_2 films were ~-3.3 and ~-5.1 V, respectively. The absolutely higher forming voltage for the c-HfO_2 film must be related with the presence of interfacial TiON layer as well as difficult migration of oxygen ions in the crystalline HfO_2 compared with amorphous HfO_2. Both samples could be reliably cycled up to ~1,000 cycles (upper panel figures in Figs. 5c, d), but further cycling was not attempted. The BRS switching I-V curves during the initial I-V sweeps up to 50 cycles are shown in Figures 5e, and f. The two samples showed quite distinctive evolutions of the switching I-V curve during the

electroforming and subsequent BRS switching operations. While a common compliance current (I_{cc}) of 5 μA was adopted during the electroforming, the peak current immediately prior to the switching to HRS in the positive bias region during the subsequent reset sweep reached ~20 mA at the reset voltage (V_{reset}) of ~2.8 V for the a-HfO_2 film. In contrast, the c-HfO_2 film showed a much smaller maximum current (~70 μA) during the subsequent first reset step, which occurred at the V_{reset} of 4.8 V. The current of the a-HfO_2 film decreased by ~3 orders of magnitude after the reset, but that of the c-HfO_2 film decreased only three to four times. A similar difference was observed in the subsequent set switching in the negative bias region. The a-HfO_2 film showed a current jump to 1 mA, which was I_{cc} for set switching, at the set voltage (V_{set}) of ~-3.0 V. The c-HfO_2 film showed set switching, however, at ~-2.4 V, but the current level after the set occurrence remained at only several tens of μA, resulting in a much lower resistance ratio between the HRS and LRS compared with the a-HfO_2 film. It should be noted that no I_{cc} was applied for the set switching in this case, which could be more clearly observed in Fig. 5f. This could be considered as a self-compliance behavior of this sample which is usually related with the presence of serial resistance component in the circuit or sample itself. As will be discussed in detail in subsequent section dealing with the IS, the resistance switching in c-HfO_2 occurs only at a certain portion of local conducting path while other parts of the path constitute a high serial resistance component which remained rather invariant during the repeated switching cycles.

The repeated BRS operation generally decreased the V_{reset} and V_{set} for both samples, but the trend of the variations in the set and reset current levels was quite different. For the a-HfO_2 film, the current in the LRS and HRS in both bias polarities generally decreased and increased, respectively, with the number of BRS cycles, making the resistance contrast decrease. As can be understood from the upper panel of Figure 5c, however, which shows the endurance performance of the a-HfO_2 film, the resistance ratio of this sample was still as high as ~500 even after 1,000 cycles. In contrast, the c-HfO_2 film showed a general increase in the currents for both the LRS and HRS, with the increasing BRS cycles during the first 50 cycles, and then they became quite invariant, making the resistance ratio stably stay at ~7 during the whole endurance test (upper panel of Figure 5d). Another critical feature of the c-HfO_2 film was its exceptionally small switching voltages (V_{set} ~-0.2 V, V_{reset} ~0.4 V), which resulted in a smaller reset switching power of ~0.4 mW compared with that of the a-HfO_2 film (~1.4 mW). The I-V curves after ~50 BRS cycles are stabilized and no further variations were observed. The lower panels of Figures 5c, d show the retention characteristics of the two samples measured at 80°C. Both samples showed sufficient stability in the resistance states for RRAM application. The direct current (DC) I-V test revealed that the c-HfO_2 film has several important merits over the a-HfO_2 film in terms of the switching power, uniformity, and retention. Its small resistance ratio (<10), however, can pose problems for mass production considering the die-to-die and wafer-to-wafer variations. In contrast, the a-HfO_2 film showed fluent BRS performances, but its larger variation could

be problematic. Such difference in the RS characteristics of the two samples could be understood from the fact that the c-HfO_2 film had a highly resistive component whose resistance state remained invariant during repeated switching, and that only a minor portion of the sample underwent BRS. In contrast, in the case of the a-HfO_2 sample, a major portion of it underwent changes in the resistance state, making the resistance contrast higher but the uniformity lower. Using the IS in the subsequent section, what actually governs such variations in the two samples was examined.

Ln I vs. Ln V plot of the a-HfO_2 and Ln (J/E) vs. $E^{1/2}$ c-HfO_2 samples are shown in Figure 6a, b to determine the conduction mechanisms in LRS and HRS. When positive bias was applied to TE (Figure 6a), the current flowed in an Ohmic way in a low-voltage region (< ~0.3 V) while it flowed according to the space charge limited current (SCLC) mechanism in a high-voltage region for the LRS of the a-HfO_2 sample. This must be a reasonable consequence considering that the a-HfO_2/TiN BE maintains low resistance contact, making the carrier injection excessive at a high-voltage region, so that the injected carriers trapped by the high density of oxygen vacancies in the region near the a-HfO_2/Pt interface and SCLC was induced. On the other hand, the Ohmic current flowed when the injection was not excessive at lower voltages. In HRS, the a-HfO_2 sample showed Poole-Frenkel-type characteristics (Figure 6b), suggesting that the a-HfO_2/Pt interface region recovered a high SB but still contained an appreciable density of defects (oxygen vacancies). For the c-HfO_2 sample, the followings were observed from the DC transport characteristics analysis. In the Ln I vs. Ln V plot for LRS (Figure 6c), the current shows a linear relation with a slope of ~1, suggesting an Ohmic conduction. For HRS (Figure 6d), the current flowed in an Ohmic way in a low-voltage region (<~0.3 V), but at a high-voltage region, the current followed the relation $I \propto V^2$ (Child's law). This suggests that the HRS of the c-HfO_2 film can be described using the SCLC mechanism. These DC conduction mechanisms could be well correlated with the microstructural change in the two samples according to the resistance states, which were elucidated by the IS described below.

Impedance analysis

Figures 7a-c show the evolution of AC IS for the electroforming in the negative bias voltage region, first reset in positive bias voltage, and subsequent set in the negative bias voltage region of the a-HfO_2 sample in a three-dimensional plot. Each IS was obtained after DC I-V sweep was performed to each DC bias voltage indicated in the bottom plane of the three-dimensional Cole-Cole-type plot, and the next IS at a higher voltage was acquired after the samples were swept again from 0 V to the desired DC voltage. Here, the DC voltage step for the different IS was 0.4 V. The figures in the lower panel with numbers highlight the characteristic changes observed in the IS during the DC I-V sweep. The pristine a-HfO_2 sample before the electroforming (Figure 7a, panel 1-3) showed an IS typical to a

highly insulating MIM. The sample had a very high combined capacitance and resistance (R'C) component almost in the whole frequency range (0.1-5x10^6 Hz), which must be related to the high depletion capacitance and high resistance of the a-HfO_2/Pt interface region. R' was too high to be quantitatively estimated in this IS setup. In very-high-frequency region (6x10^6-1x10^7 Hz), the IS revealed a combined resistance and inductance (R"L") where the R" was much lower (~130 Ω) than R', which is ascribed to the contact resistance between the a-HfO_2 film and the TiN BE. The involved L" (inductance) component with R" can be ascribed to the small polarization due to the presence of oxygen ions at that interface.[21] After the occurrence of electroforming, the IS showed a drastic change, as shown in panel 4 of Figure 7a. The high R'C' component in the low-frequency region disappeared, and only the R"L" component in the high-frequency region remained. The disappearance of the high R' component after the electroforming well coincides with the DC I-V sweep results shown in Figure 5a, suggesting that the high and thick SB at the a-HfO_2/Pt interface disappeared due to the loss of oxygen ions. Interestingly, R" slightly increased to ~180 Ω and the L" component became more obvious (the clearer semi-circle in the negative Z' region) even though the sample was electroformed. This implies that the a-HfO_2/TiN interface comes to have a slightly higher contact resistance, and that the interfacial polarization also slightly increases through the trapping of more oxygen ions. Such variations in IS during the electroforming well coincides with the idea that the oxygen ions of the a-HfO_2/Pt TE interface region drifted towards the TiN BE, and that most of the oxygen ions came to be contained within the TiN while a few of them came to reside at the interface region.

When the positive bias was subsequently applied to induce the first reset, the variations in IS were quite simple, as shown in Figure 7b. The IS maintained in the electroformed state until the reset voltage was reached (panels 1-3 of Figure 7b), and sudden changes were observed after reset. After reset, the IS showed a typical R'C component in a wide frequency range (0.1-5x10^6 Hz) with the R' value of ~4 MΩ, which implies that a substantial number of the oxygen ions drifted to the TiN BE (and also to the interface) moved back to the a-HfO_2/Pt interface region, recovering the SB, but the recovered SB was certainly weaker than that in the pristine state. After the reset, the R" component decreased again to the initial value (~130 Ω, panel 4 in Figure 7b), with lower polarization-related inductance, suggesting that the a-HfO_2/TiN interface went back to the pristine state. This reveals that the trapping of oxygen ions at the interface with the TiN BE during electroforming was rather weak, making the trapping (during the electroforming and set) and detrapping (during reset) repeatable. When the negative bias was subsequently applied to set again the a-HfO_2 sample, the IS showed complicated variations before actual setting occurred. At a low negative bias voltage (-0.4 V), the R' value in the low-frequency region temporarily decreased to ~3 MΩ while the R" in the high-frequency region increased to ~280 Ω (panel 1 in Figure 7c). This means that some of the oxygen ions in the a-HfO_2/Pt interface region started to move towards the TiN BE, but some of them were trapped at the

interface with the TiN BE, at such a low bias voltage. When the bias was further increased in the negative bias direction (panels 2-3 in Figure 7c) the IS became quite similar to that of the pristine state in the higher-frequency region (R" ~130 Ω), and the R' in the low-frequency region recovered that of the reset state (~4–5 MΩ). This suggests that the oxygen trapped at the a-HfO_2/TiN interface was detrapped and moved into the TiN BE through the increased bias voltage, and that the a-HfO_2/Pt interface region started to gain oxygen ions from the atmosphere that were diffused through the Pt TE. Such tendency became even more obvious as the bias further increased negatively. R' finally increased to ~8 MΩ immediately prior to the setting actually occurs. After the setting, the high R' component disappeared (panel 4 of Figure 7c), suggesting that the high and thick SB disappeared again due to the oxygen movement towards the TiN BE, while R" again increased to ~200 Ω. The IS at this stage, however, was slightly different from that of the as-electroformed state (panel 4 of Figure 7a), which is consistent with the fact that the V_{set} and electroforming voltage (or set and electroforming powers) are different. It is interesting to note that the tendencies of change in R' and R" during the first reset and set processes are opposite once the sample is electroformed. R' increases from almost zero to several MΩ while R" decreases slightly at the moment of resetting. In contrast, R' decreases abruptly from several MΩ to almost zero while R" increases slightly at the moment of setting. This can be understood from the reversed tendency of gain and loss of the oxygen ions of the a-HfO_2 sample near the Pt TE and TiN BE. These observations on the physical status of the LRS and HRS in a-HfO_2 sample well corresponds to the DC conduction mechanism mentioned in Figs. 6 a and b; SCLC in LRS coincides with the excessive carrier injection and partial trapping of them along the conducting path, while the recovered SB in the HRS suppressed the carrier injection and trapping/detrapping of injected carriers within the space charge region of the SB coincide with the Poole-Frenkel mechanism.

Compared with the a-HfO_2 sample, the variations in IS during the electroforming, resetting, and setting of the c-HfO_2 sample are much more complicated. Figure 8a reveals that the pristine c-HfO_2 sample also had two different relaxation time constants corresponding to the c-HfO_2/Pt and c-HfO_2/TiN interfaces. When the negatively applied voltage was lower than ~-1 V, the R'C' component in the low-frequency region (0.1-10^6 Hz) was over the measurement limit of the setup corresponding to the highly insulating state of the pristine sample. The estimated R" from the IS in the high-frequency region (10^6-10^7 Hz), however, which represents the contact property between the c-HfO_2 sample and the TiN BE, was much higher (~1.3 kΩ) than that of the a-HfO_2 sample (~130 Ω) (panel 1 in Figure 8a), and the IS at the bias voltages of -0.8 and -1.6 V had a shape in between those of the R"C" (panels 2 and 3 in Figure 8a) components. This well coincides with the XPS depth profile (Figure 3b) and TEM results (Figure 4), which show that the c-HfO_2/TiN interface had a TiON layer, which must have induced the high contact resistance. When negative bias voltages of from -1.6 V to -

4.8 V were applied, the IS in the low-frequency region came to have an obvious R"C" semi-circle with a much higher R" value while the very high R'C' component hardly showed any change. This suggests that the sample remained in the highly insulating state. The R" was ~200 kΩ at the bias voltage of -1.6 V, which decreased to ~100 kΩ when the bias voltage was further negatively increased to -2.4 ~ -3.2 V. This means that some of the oxygen ions migrated from the TiON layer into the TiN BE below the TiON layer. When the bias voltage was further negatively increased to ~-5.1 V, an interesting variation in IS was observed in the middle-frequency range. A small but evident semi-circle with a resistance (R^*) value of ~70 kΩ emerged while the very high R' was still retained and R" increased to ~300 kΩ. When electroforming occurred at ~-5.1 V, the very high R' disappeared, but the overall resistance of the c-HfO_2 sample remained as high as ~370 kΩ because of the retained R" and R^*. This well coincides with the DC I-V sweep results shown in Figure 5b, where the current remained at quite a low level even after the electroforming. This suggests that the interfacial TiON layer in the c-HfO_2 sample was in fact strengthened rather than weakened during the electroforming step.

The important structural differences of the c-HfO_2 film from the a-HfO_2 film are the presence of a TiON barrier layer and improved crystalline quality of non-oxidized TiN grains in the former, which substantially suppresses the drift of oxygen ions from the c-HfO_2 film into the TiN, and the presence of grain boundaries in the c-HfO_2 layer. The presence of grain boundaries induces the electrical current flows mainly along the highly localized region at the grain boundaries (CAFM in Figure 2). Thus, the drift of oxygen ions in the c-HfO_2 film occurs mostly along the grain boundaries due to the localized Joule heating effect, which can be expected from the CAFM results shown in Figure 2d. Therefore, the application of negative electroforming bias up to -5.1 V actually results in the redistribution of oxygen ions from the c-HfO_2/Pt interface region to the TiON barrier region mainly along the grain boundaries. Very high R' up to this stage revealed, however, that this oxygen redistribution was still not extensive probably due to the presence of the TiON barrier layer. In the meantime, oxygen diffusion into the c-HfO_2 film from the atmosphere, especially near the grain boundary region through the Pt TE, can occur, which further interferes with the electroforming. This may explain the emergence of the intermediate resistance (R^*) immediately next to the electroforming. These extra oxygen atoms seem to be rather strongly "stuffed" inside the c-HfO_2 as can be understood from the generally high resistance of the sample even when the sample was switched to LRS again. When the negative bias voltage was between -2.4 and -3.6 V, the oxygen ions near the grain boundaries of the c-HfO_2 film were further dragged towards the TiON, making the grain boundary region less resistive and causing it to have a resistance value of ~70 kΩ. The strong SB at the interface between the c-HfO_2 film and Pt, however, was retained at this stage, but it will eventually be broken down at an even higher negative voltage (~-5.1 V). As shown in panel 4 of Figure 8a, therefore, the

electroformed state is composed of two serially connected rather-high-resistance components, R" and R^*. As electroforming occurs only near the grain boundary regions of the c-HfO_2/Pt interface, only a small amount of oxygen ions migrates at the moment of electroforming, and the R" and R^* can remain only minimally influenced. Due to the barrier property of the TiON layer against the drift of oxygen ions into the TiN BE, some of the drifted oxygen ions could be diffused into the neighboring HfO_2 bulk grains.

When the bias voltage was reversed to the positive side to reset the c-HfO_2 sample (Figure 8b), the sample state remained quite invariant up to a voltage of ~4 V, and the IS showed that the two serial components, R" and R^*, remained unchanged (panels 1-3 of Figure 8b). When the bias voltage increased to ~4.5 V, reset occurred in DC I-V (Figure 5b), and the IS at this stage clearly revealed what happened at this step (panel 4 of Figure 8b). The R" remained almost unaltered, meaning that the TiON barrier layer remained invariant even after the reset, but the R^* value appeared to increase to ~130 kΩ, so that the total resistance came to be ~430 kΩ. There was no recovery of R', which was not the case for the a-HfO_2 sample, and as such, the samples were much more conducting even after the reset compared with the pristine state. This means that in the c-HfO_2 film, the reset is nothing but the (partial) refilling of oxygen vacancies along the grain boundaries with the oxygen ions supplied from the TiON or other trapped oxygen ions at the TiON/c-HfO_2 interface, or even from the nearby HfO_2 grains. This also implies that the supply of additional oxygen through Pt electrode during the later cycles of switching did not occur. These observations on the physical status of the LRS and HRS in c-HfO_2 sample well corresponds to the DC conduction mechanism mentioned in Figs. 6 c and d; the generally high overall resistance of the c-HfO_2 due to the presence of TiON layer limits the carrier injection even in LRS so that Ohmic conduction can be observed in wide voltage region. When the sample was in HRS, the carrier injection was slightly further suppressed but trapping/detrapping mediated conduction mechanism, such as Poole-Frenkel, was not induced since the SB was not recovered in this case. Only SCLC mechanism could be observed when the bias voltage was high.

Upon the reverting of the bias polarity to negative to set the c-HfO_2 sample, notable changes were observed only for the R^* component; the R" component remained invariant. When the negative bias voltage became lower than ~-2.5 V, R^* shrunk to ~70 kΩ (panel 4 of Figure 8c), and the overall resistance also decreased to ~370 kΩ. The overall change in resistance, therefore, must have been small in this case, making the resistance ratio between the LRS and HRS of the c-HfO_2 film quite smaller than that of the a-HfO_2 film, which is primarily ascribed to the fact that R" was invariantly present throughout the whole RS. It must be noted that the electrical response in the IS could also have been contributed by the non-active part of the sample (the grain area in the c-HfO_2 film, which is believed to be mostly inactive during the whole RS) so that the resistance ratio in the AC IS (430/370) was much smaller than that in the DC I-V case (~7). It must be instructive to see that AC IS can reveal

the type of changes that occur in the HfO_2/Pt and HfO_2/TiN interfaces separately, which will enable the precise understanding of what the DC bias voltages induce inside the material. The very small switching voltage after the switching cycles of ~ 50 in c-HfO_2 (Fig. 5f) coincides well with the IS results. IS revealed that only small portion of the material, especially along the grain boundaries, contributes to the actual switching in this case due to the presence of TiON barrier layer and no recovery of Schottky barrier at the interface with Pt electrode. If the length of this active switching portion is assumed to be 2 nm, the switching voltage of 0.2 V corresponds to a switching field of 1 MV/cm, which is still high enough to induce the ion drift in that very local region.

The crystallized microstructure of the c-HfO_2 film induced the spatially localized current flow along the grain boundaries while the uniform microstructure of the a-HfO_2 film resulted in a more uniform current flow especially in HRS. Therefore, it is believed that the RS in the a-HfO_2 film occurs over a wider area than that in the c-HfO_2 film. It must be noted that there could be more and less active (or even almost non-active) areas even in the a-HfO_2 film. It is obvious, however, that the relative portion of the active area to the non-active area must be higher for the a-HfO_2 film than for the c-HfO_2 film. The LRS and HRS resistance values of a-HfO_2 and c-HfO_2 samples with different electrode areas ($5x10^3$ – $1x10^6$ μm^2) measured at 0.1V using DC I-V sweep showed that both samples have localized conducting channels meaning that the interface area type switching does not occur in a-HfO_2 (Inset figures in Figs. 5a and b). The LRS resistance values of a-HfO_2 and c-HfO_2 samples showed absolutely no area-dependency, while HRS resistance values showed slight area-dependency (resistance varied by ~ 1 order of magnitude when area varies by 2.5 orders of magnitude for a-HfO_2, and ~0.5 orders of magnitude for the same area variation for c-HfO_2). Therefore, the switching mechanism identified from the IS should be interpreted as being occurred at local spots in both types of samples. Summary of various R components during the first cycle of switching are given in table I. It must be noted that there could be (partial) crystallization of the a-HfO_2 during the repeated switching cycles due to the Joule heating effect especially near the more conducting (local) path region. Even with such possibility, the absence of interference effect for oxygen migration due to the lack of interfacial TiON barrier layer does not suppress the fluent switching in this case. There could be two cases in the relative locations between the grain boundaries of c-HfO_2 and TiN; they are coincident and disparate. In the former case, the TiON at grain boundaries of TiN blocks the oxygen migration along the c-HfO_2 grain boundaries. In the latter case, the improved crystallinity of TiN would suppress the oxygen migration into the TiN. For the latter case, the oxygen might diffuse along the interface between the c-HfO_2 and TiN grains to the grain boundaries where the TiON presents. In either case, the oxygen migration must be suppressed.

IV. Conclusion

In conclusion, the BRS behaviors of Pt/a-HfO_2/TiN and Pt/c-HfO_2/TiN were examined using DC I-V sweep and AC IS. The IS of the a-HfO_2 film showed that the interfacial resistance with the TiN BE in the pristine state was quite low (~130 Ω), which remained relatively unaltered throughout the whole BRS cycle. This is consistent with the observation that the TiN/HfO_2 interface hardly bore any interfacial oxide layer. When the negative bias was applied for the electroforming, the oxygen atoms in the a-HfO_2 layer fluently moved into the TiN BE as there was no barrier layer. When the density of the oxygen vacancies near the Pt BE became high enough to lower the SB height and width, fluent carrier injection occurred, and the sample came to be in LRS. When the bias polarity was reversed into the positive direction, the electron injection at the TiN/HfO_2 was fluent, and the lowered SB at the Pt TE interface did not interfere with the electron transport, thus maintaining the LRS even in the positive bias region as long as the positive bias was lower than the V_{reset}. When the bias voltage increased to over the V_{reset}, oxygen atoms were drifted from the TiN BE to the interface region with the Pt TE recovering the height and width of SB. This was not interfered by the absence of a TiON barrier layer. A certain amount of oxygen atoms during the repeated set and reset processes, however, can be progressively trapped at the TiN/HfO_2 interface. This reduces the LRS current because it works as a higher contact resistance, while the HRS current could be increased as the recovery of the SB barrier at the a-HfO_2/Pt interface could be less effective due to the loss of oxygen ions owing to the trapping. Therefore, such oxygen trapping generally decreases the current ratio of LRS and HRS, with increasing RS cycle number, which can be seen in Figure 6a.

The c-HfO_2 sample can be most evidently characterized as having an interfacial TiON layer, which works as a barrier layer for the oxygen migration between the c-HfO_2 film and TiN BE and increases the contact resistance even in the pristine state, and improved crystalline quality of non-oxidized TiN grains which also contributes to the suppression of oxygen drift. In addition, the current must flow mostly along several spatial locations at the grain boundaries. Even though the Pt/c-HfO_2 interface has high and thick SB at the pristine state, it disappears once the c-HfO_2 is electroformed and was not recovered even after the reset step at the locations where the most conducting grain boundaries are present. This makes the LRS/HRS current ratio generally small and limits the switching region to a certain portion of the conducting paths over the grain boundaries. The switching during the repeated BRS operations after the electroforming was attributed to the filling and emptying of the conductive grain boundaries with oxygen ions. The generally increasing LRS and HRS currents with the increasing BRS cycles (Figure 5f) suggest that the TiON barrier was generally weakened by the electrical stresses. The very small switching voltages ($<<$ 0.5 V) after many switching cycles indicates that the switching region is highly spatially restricted to only several local spots along the grain boundaries, which is favorably related to the very uniform switching parameters.

Acknowledgments

JHL acknowledges support from SK Hynix Semiconductor Inc. and National Research Foundation (NRF) of Korea (grant no. 2013R1A2A101006545). CSH acknowledges the support of Global Research Laboratory program (2012040157) through the National Research Foundation (NRF) of Korea.

References

1. G. D. Wilk, R. M. Wallace, J. M. Anthony, *J. Appl. Phys*. **2001**, *89*, 5243.

2. P. Gonon, M. Mougenot, C. Vallee, C. Jorel, Jousseaume, H. Grampeix, F. El Kamel, *J. Appl. Phys*. **2010**, *107*, 074507.

3. B. Govoreanu, G. S. Kar, Y. -Y. Chen, V. Paraschiv, S. Kubsek, A. Fantini, I. P. Radu, L. Goux, S. Clima, R. Degraeve, N. Jossart, O. Richard, T. Vandeweyer, K. Seo, P. Hendrix, G. Pourtois, H. Bender, L. Altimine, D. J. Wouters, J. A. Kittl, M. Jurczak, *Int. Electron. Dev. Meet. Tech. Dig*. **2011**, 729.

4. H. Y. Lee, P. S. Chen, T. Y. Wu, C. C. Wang, P. J. Tzeng, C. H. Lin, F. Chen, M. -J. Tsai, C. Lien, *Appl. Phys. Lett*. **2008**, *92*, 142911.

5. M. Y. Chan, T. Zhang, V. Ho, P. S. Lee, *Microelectron. Eng*. **2008**, *85*, 2420.

6. D. -H. Kwon, K. M. Kim, J. H. Jang, J. M. Jeon, M. H. Lee, G. H. Kim, X. -S Li, G. -S. Park, B. R. Lee, S. W. Han, M. Y. Kim, C. S. Hwang, *Nat. Nanotechnol*. **2010**, *5*, 148.

7. B. J. Choi, D. S. Jeong, S. K. Kim, C. Rohde, S. Choi, J. H. Oh, H. J. Kim, C. S. Hwang, K. Szot, R. Waser, B. Reichenberg, S. Tiedke, *J. Appl. Phys*. **2005**, *98*, 033715.

8. M. Lanza, K. Zhang, M. Porti, M. Nafia, Z. Y. Shen, L. F. Liu, J. F. Kang, D. Gilmer, G. Bersuker, *Appl. Phys. Lett*. **2012**, *100*, 123508.

9. V. Iglesias, M. Lanza, A. Bayerl, M. Porti, M. Nafria, X. Aymerich, L. F. Liu, J. F. Kang, G. Bersuker, K. Zhang, Z. Y. Shen, *Microelectron. Reliab*. **2012**, *52*, 2110.

10. F. De Stefano, M. Houssa, J. A. Kittl, M. Jurczak, V. V. Afanas'ev, A. Stesmans, *Appl. Phys. Lett*. **2012**, *100*, 142102.

11. D. Ielmini, *IEEE T. Electron. Dev*. **2011**, *58*, 4309.

12. S. Yu, R. Jeyasingh, Y. Wu, H. -S. Philip Wong, *Appl. Phys. Lett*. **2011**, *99*, 232105.

13. L. Goux, P. Czarnecki, Y. Y. Chen, L. Pantisano, X. P. Wang, R. Degraeve, B. Govoreanu, M. Jurczak, D. J. Wouters, L. Altimime, *Appl. Phys. Lett*. **2010**, *97*, 243509.

14. S. Balatti, S. Larentis, D. C. Gilmer, D. Ielmini, *Adv. Mater*. **2013**, *25*, 1474.

15. J. S. Kwak, Y. H. Do, Y. C. Bae, H. S. Im, J. H. Yoo, M. G. Sung, Y. T. Hwang, J. P. Hong, *Appl. Phys. Lett*. **2010**, *96*, 223502.

16. H. K. Kim, S. Y. Lee, I. -H. Yu, T. J. Park, R. N. Choi, C. S. Hwang, *IEEE Electron Dev. Lett*. **2012**, *33*, 955.

17. D. S. Jeong, H. Schroeder, R. Waser, *Appl. Phys. Lett*. **2006**, *89*, 082909.

18. X. L. Jiang, Y. G. Zhao, Y. S. Chen, D. Li, Y. X. Luo, D. Y. Zhao, Z. Sun, J. R. Sun, H. W. Zhao, *Appl. Phys. Lett*. **2013**, *102*, 253507.

19. Y. -H. You, B. -S. So, J. -H. Hwang, W. Cho, S. S. Lee, T. -M. Chung, C. G. Kim, K. -S. An, *Appl. Phys. Lett*. **2006**, *89*, 222105.

20. Sarma D. D., Rao C. N. R., *J. Electron Spectrosc. Relat. Phenom*. **1980**, *20*, 25.

21. M. Bojinov, S. Cattarin, M. Musiani, B. Tribollet, *Electrochim. Acta* **2003**, *48*, 4107.

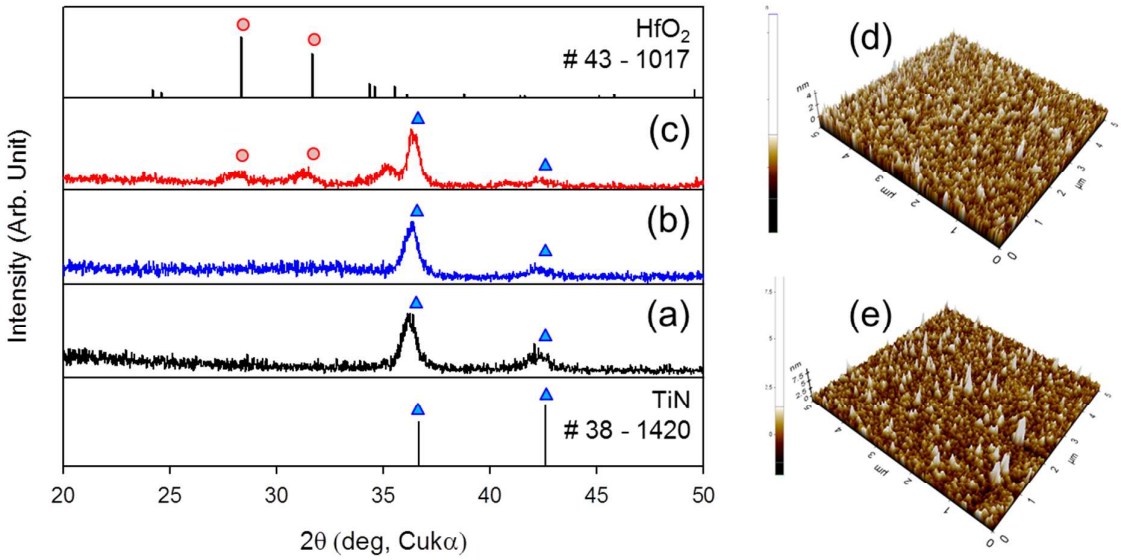

Figure 1. X-ray diffraction patterns of thin films deposited on SiO_2/Si substrate. (a) TiN, (b) as-deposited HfO_2 and (c) HfO_2 heat-treated at 500°C for 5 minutes, and topographic AFM images of the 11.3-nm-thick (d) a-HfO_2 and (e) c-HfO_2 films.

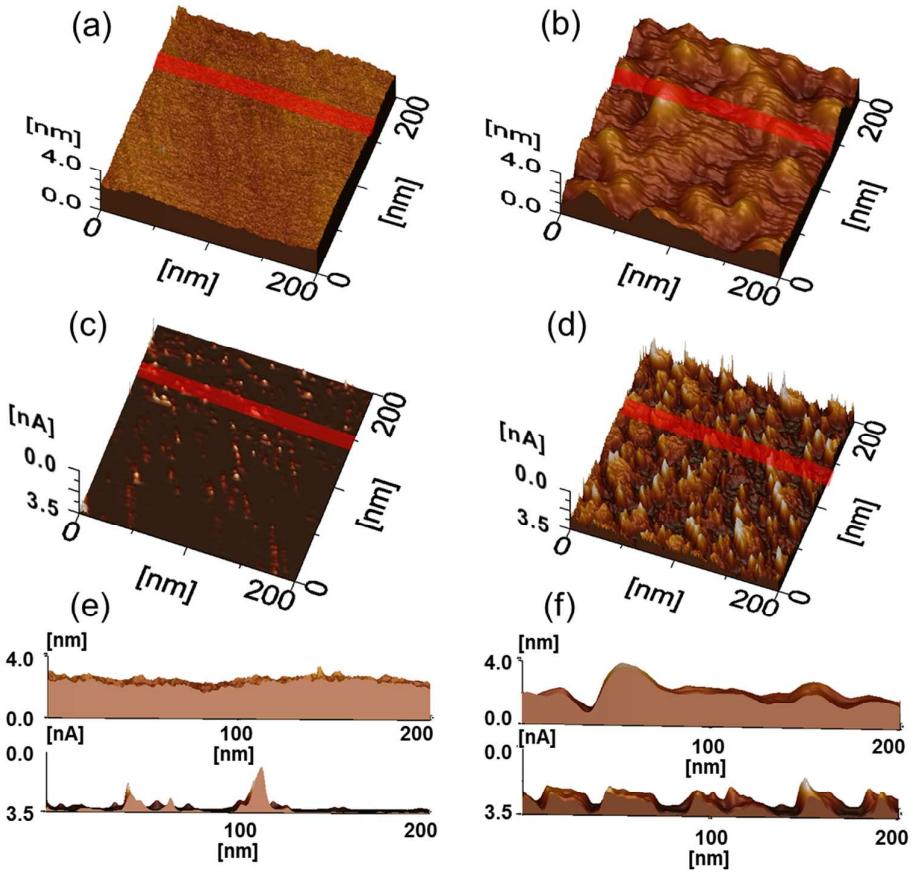

Figure 2. Topographic AFM images of 5.5-nm-thick (a) a-HfO_2 and (b) c-HfO_2 films, and CAFM images of the (c) a-HfO_2 and (d) c-HfO_2 films. (e) and (f) show the cross-section images of (c) and (d) indicated by red-colored band. Note that the deeps in (e) and (f) correspond to the high current locations.

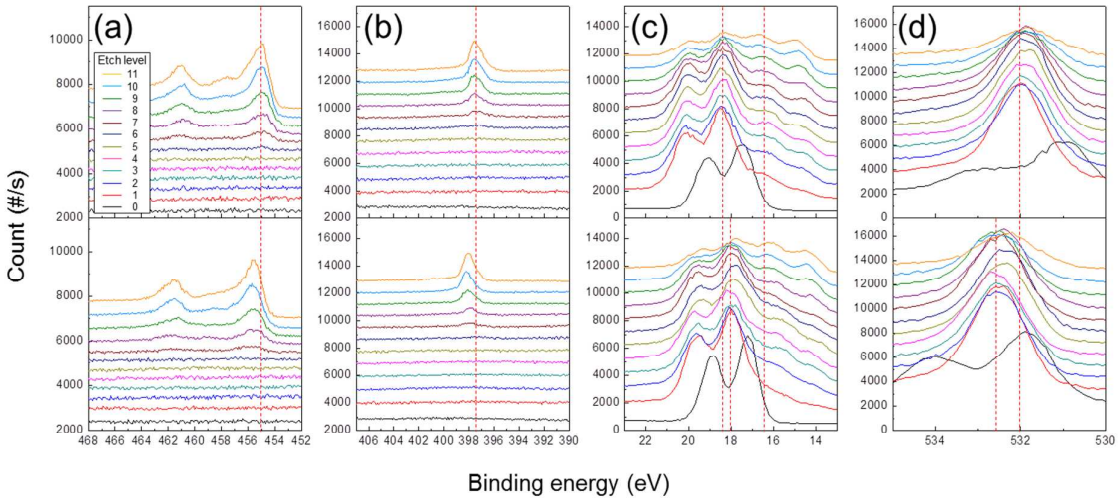

Figure 3. X-ray photoelectron spectroscopy depth profile results of (a) Ti *2p*, (b) N *1s*, (c) Hf *5f* and (d) O *1s*; a-HfO_2 (top panels) and c-HfO_2 (bottom panels). Vertical dashed lines are guide to eyes. There are certain discrepancies in the binding energies of the peaks between the amorphous and crystalline HfO_2 films.

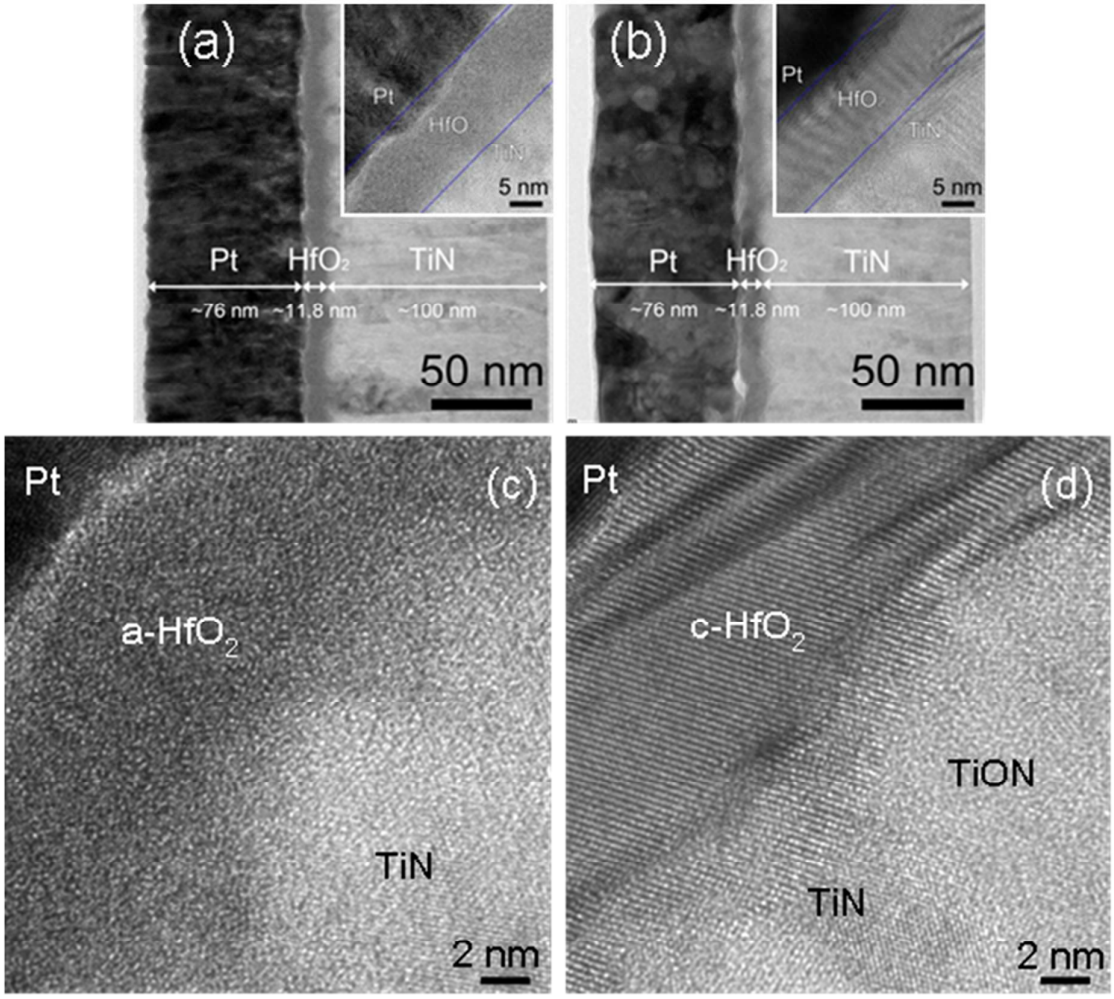

Figure 4. Cross-sectional TEM images of (a), (c) a-HfO_2, and (b), (d) c-HfO_2 samples. (a, b) low magnification (inset: medium magnification), and (c, d) high-resolution images. c-HfO_2 sample often shows amorphous-like structures, which is believed to be TiON, between crystalline TiN grains at the c-HfO_2/TiN interface (d), while a-HfO_2 sample barely showed distinctive amorphous-like structures at the a-HfO_2/TiN interface (c).

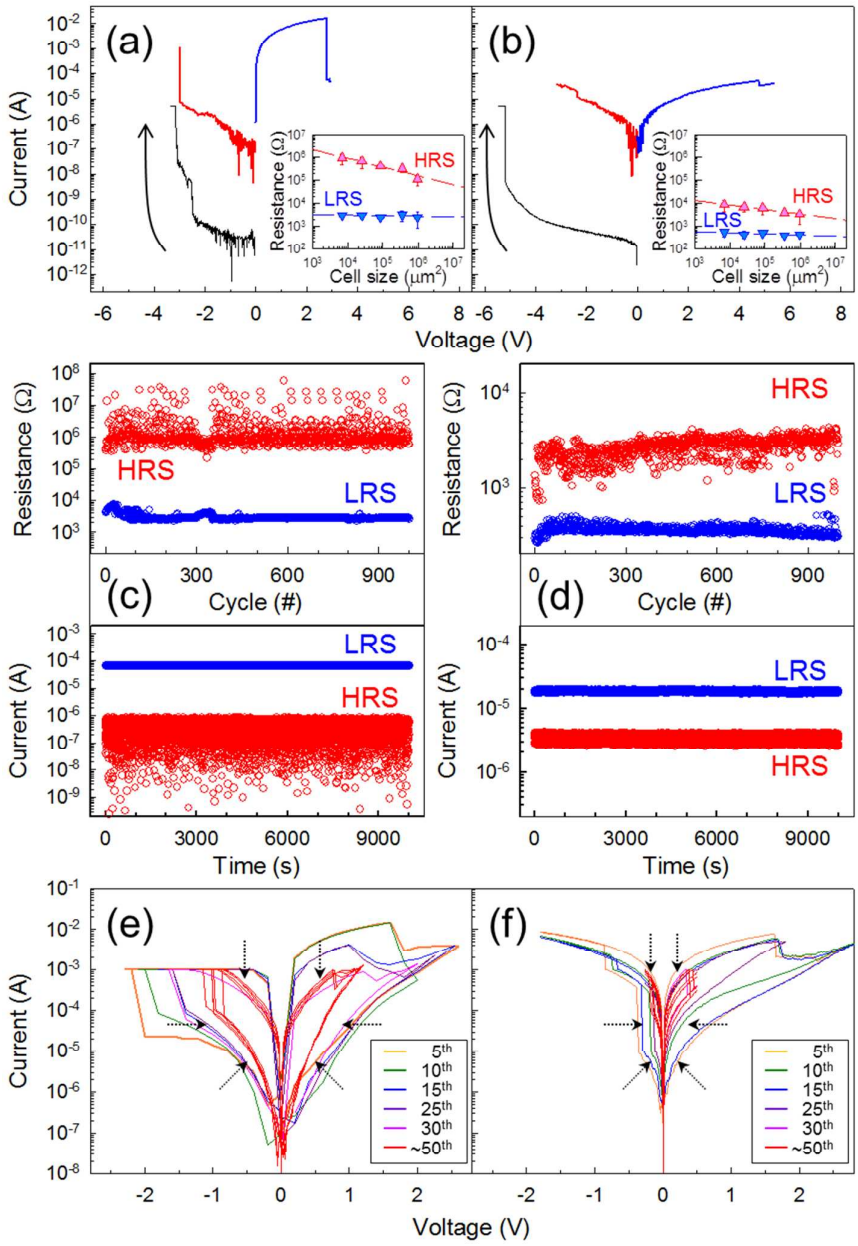

Figure 5. DC I-V curves of (a) a-HfO_2 and (b) c-HfO_2 from pristine state to 1st set. The endurance performance (upper panel) and retention test (lower panel) results (measured at 0.1V for a-HfO_2 and 0.02V for c-HfO_2) of (c) a-HfO_2 and (d) c-HfO_2. The endurance was measured by DC sweep. Evolution of current-voltage curves of (e) a-HfO_2 and (f) c-HfO_2 during endurance test. Cycling results up to 50 cycles are shown, and I-V curves afterwards did not show notable changes. Inset figures in (a) and (b) show the area-dependency of HRS and LRS resistances.

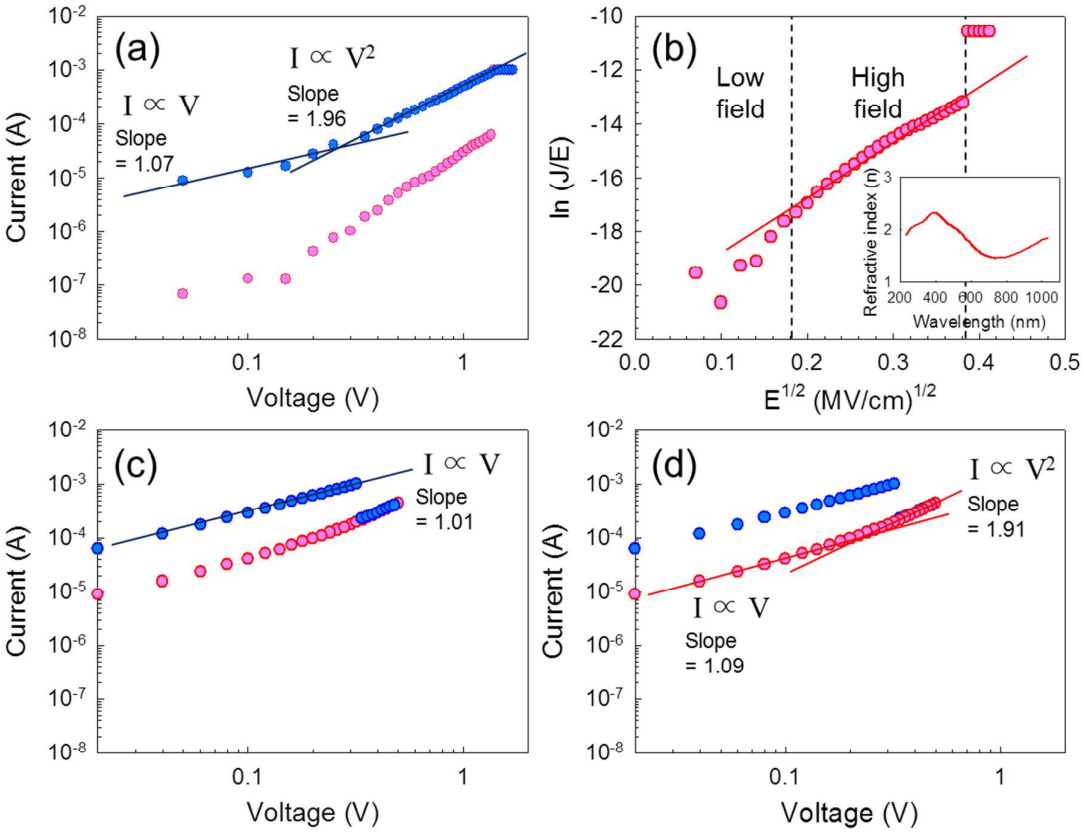

Figure 6. (a) DC I-V curves plotted on a log-log scale for LRS and HRS of the a-HfO_2, (b) a plot of ln(J/E) against $E^{1/2}$ for the a-HfO_2 in HRS. The inset of Figure 6(b) shows the measured refractive index of the a-HfO_2 thin film using ellipsometry. Extracted optical dielectric constant of the a-HfO_2 from the Schottky fitting was 2.18 corroborating the optical measurement data (2.14). (c) and (d) I-V curves plotted on a log-log scale for LRS and HRS, respectively, of the c-HfO_2.

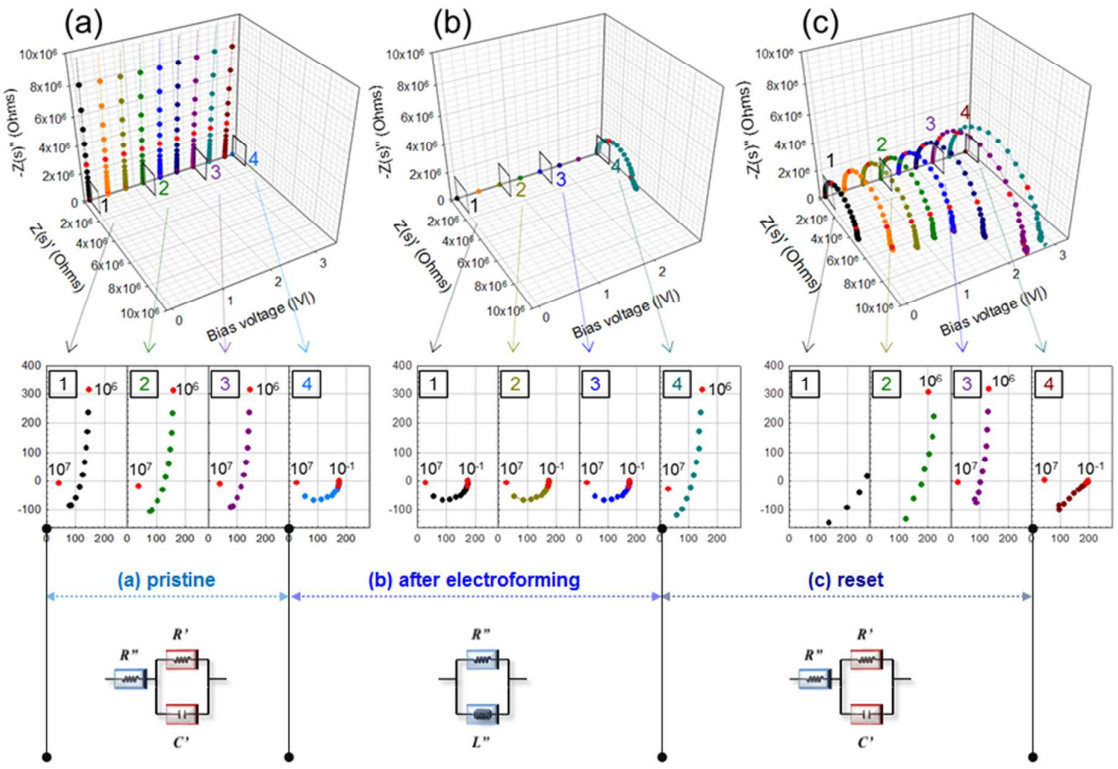

Figure 7. Evolution of complex impedance spectra of a-HfO_2 from initial state to 1st set: (a) from initial state to electroforming; (b) from electroforming to 1st reset; (c) from 1st reset to 1st set. Lower panels show the two-dimensional plots of IS indicated by the numbers in upper panels (x- and y-axis dimensions are Ohms). These panels show the enlarged spectra near origin of the small boxes in the upper panel figures. The figures below lower panel show the equivalent circuits at (a) pristine, (b) after electroforming, and (c) reset.

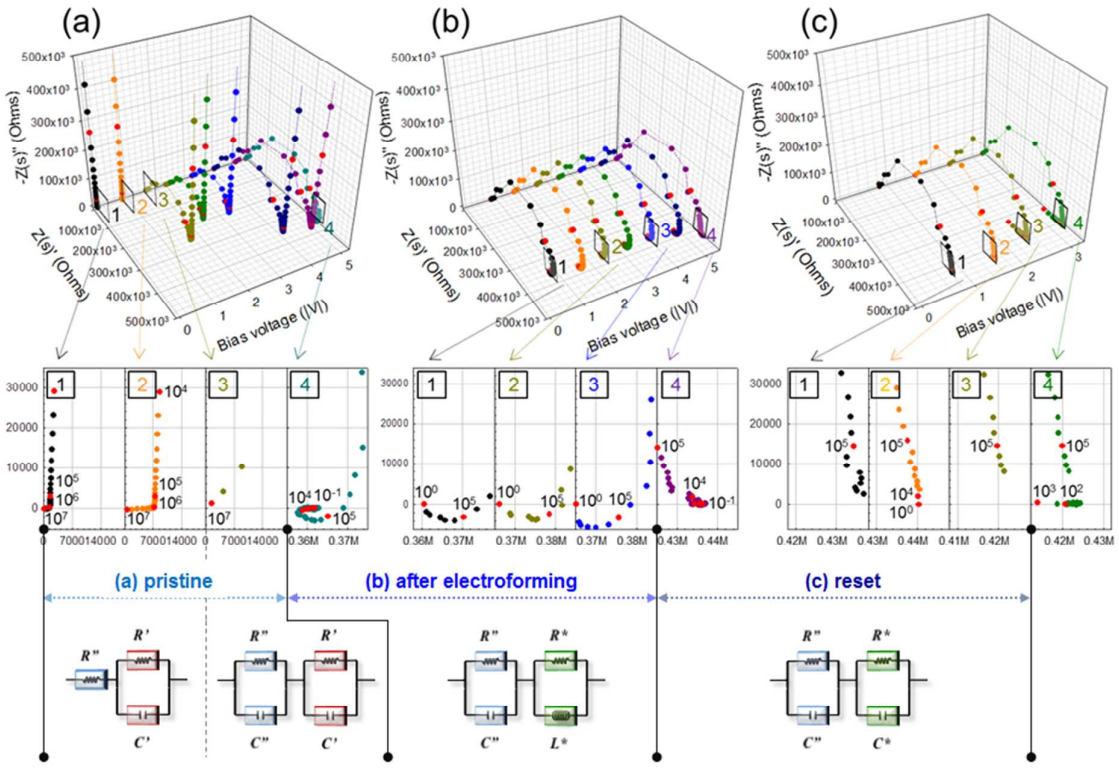

Figure 8. Evolution of complex impedance spectra of c-HfO_2 from initial state to 1st set: (a) from initial state to electroforming; (b) from electroforming to 1st reset; (c) from 1st reset to 1st set. Lower panels show the two-dimensional plots of IS indicated by the numbers in upper panels. (x- and y-axis dimensions are Ohms) **).** These panels show the enlarged spectra near origin of the small boxes in the upper panel figures. The figures below lower panels show the equivalent circuits at (a) pristine, (b) after electroforming, and (c) reset.

Table I. Resistance values of various component in a-HfO_2 and c-HfO_2 during the first switching cycle.

a-HfO_2	**Pristine**	**Electroformed**	**1st reset**	**1st set** (-0.4V)	**1st set** (-0.6 – -2.2V)	**1st set** (-2.3 - -2.8V)	**1st set** (<~ -3V)
R' (Ω)	Over range	~0	4 x 10^6	3 x 10^6	4-5 x 10^6	8 x 10^6	~0
R" (Ω)	130	180	130	280	130	130	200

c-HfO_2	**Pristine**	**Electroformed**	**1st reset**	**1st set (-2.5V)**
R' (Ω)	Over range	~0	~0	~0
R" (Ω)	1.3x10^3	3x10^5	3x10^5	3x10^5
R* (Ω)		7x10^4	1.3x10^5	7x10^4

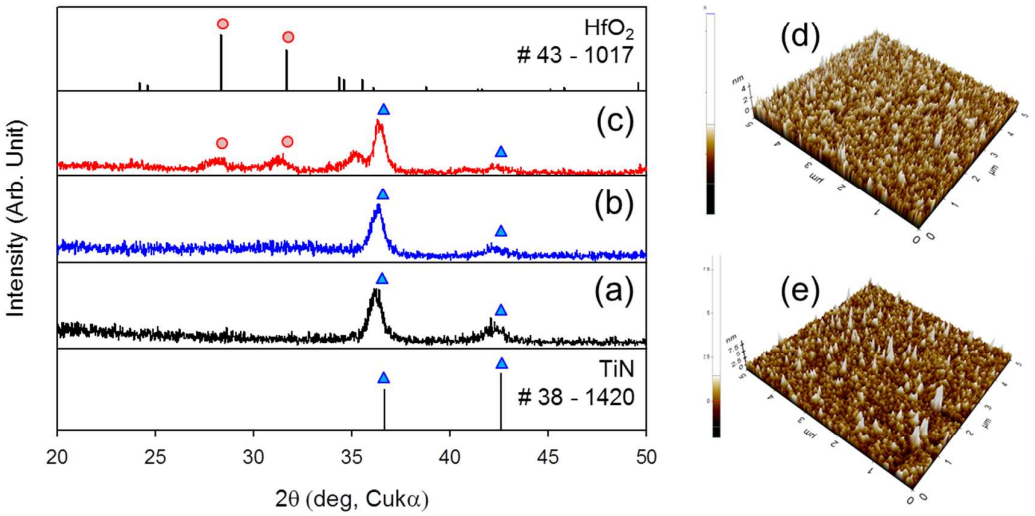

Microscopic-level changes such as the dynamic evolutions in conducting filament, interfacial TiON region, and matrix phase during various steps of resistance switching were studied using AC impedance spectroscopy.